AIAA JOURNAL
Vol. 31, No. 1, January 1993

Theoretical and Experimental Study on Two-Phase Structure of Planar Mixing Layer

Keh-Chin Chang,* Muh-Rong Wang,* Wen-Jing Wu,† and Ying-Chieh Liu†
National Cheng-Kung University, Tainan 70101, Taiwan, Republic of China

A theoretical and experimental investigation is conducted to study the two-phase turbulent structure in a planar mixing layer with polydispersed drops. Mean and fluctuating velocity components, drop number density, as well as drop size distribution were measured with nonintrusive diagnostics of the two-component phase Doppler particle analyzer. Complete initial conditions required for theoretical calculation were also provided with measurements. Theoretical investigation is made with the Eulerian-Lagrangian formulation. Turbulent dispersion effects are numerically simulated using the Monte Carlo method. The well-defined experimental data have been used to assess the accuracy of the Eulerian-Lagrangian model. The comparisons show that the theoretical predictions, based on the Eulerian-Lagrangian model, yield reasonable agreement with the experimental data.

Nomenclature

b = mixing layer width at the inlet position
$C_1C_2C_\mu$ = coefficients in turbulent model
C_D = drag coefficient
d_p = drop diameter
G = mean liquid mass flux
g = gravity
k = turbulent kinetic energy
L_e = eddy size
M = total number of computational drops passing a cell
n = number of drops represented by a computational drop
P = value of probability density function
Re = drop Reynolds number
S_ϕ = source term
$S_{p\phi}$ = source term due to interactions between gas and drops
t = time
U,u,u' = instantaneous, mean, and fluctuating streamwise velocity components
V,v,v' = instantaneous, mean, and fluctuating transverse velocity components
x = streamwise coordinate
y = transverse coordinate
Δt = integrating time step
Γ_ϕ = transport coefficient
ϵ = dissipation rate of turbulent kinetic energy
$\mu, \mu_t, \mu_{\text{eff}}$ = molecular, eddy, and effective viscosities
ρ = density
σ = coefficient in turbulent model
τ_e = turbulent eddy lifetime
τ_p = particle dynamic relaxation time
τ_r = residence time of particle in an eddy
ϕ = dependent variable

Subscripts

i = ith direction
k = turbulent kinetic energy
p = dispersed phase
ϵ = dissipation rate of turbulent kinetic energy
$-$ = vector form
∞ = sufficiently far transverse distance

Superscripts

k = kth computational drop
$-$ = mean value

Received Nov. 1, 1991; revision received June 28, 1992; accepted for publication July 6, 1992.

*Associate Professor, Institute of Aeronautics and Astronautics. Member AIAA.
†Research Assistant, Institute of Aeronautics and Astronautics.

Introduction

A PLANAR mixing layer is formed by bringing two streams of fluid at different velocities and dividing by a central plate. This well-known structure of single-phase mixing layer flow has been experimentally studied by, for example, Brown and Roshko[1] as well as Winant and Browand.[2] In addition, the turbulence models for the single-phase mixing layer flow are reasonably well developed too. For these reasons, the two-phase mixing layer flow was selected as a fundamental case so that the important issues can be clearly addressed in regard to dispersed-phase dynamics and interactions between the two phases. There have been a number of research efforts[3-11] toward the understanding of two-phase mixing phenomena. The extensive review on the background information of two-phase mixing layer flow made by Crowe et al.[11] is recommended.

There are two fundamentally different theoretical approaches generally utilized to predict the dispersed properties in two-phase flow.[11,12] One is called the Eulerian approach or two-fluid model; the other is called the Lagrangian or tracking approach. Durst[13] examined these two different approaches and showed that the Lagrangian approach has an advantage in handling the dilute flows with polydispersed size distribution, whereas the Eulerian approach is relatively computationally efficient, particularly for monodispersed two-phase flows. The comparative studies using these two approaches conducted by Mostafa and Mongia[14] as well as Adeniji-Fashola and Chen[15] also came to similar conclusions.

Crowe et al.[11] further categorized the numerical approaches as the time-averaged and time-dependent methods. Currently the most popular time-averaged method for predicting dispersed properties in turbulence is the Monte Carlo [or the stochastic separated flow[12] (SSF)] method in which the turbulent field is represented by a random number generator. The time-dependent methods were mainly developed by Crowe's group at Washington State University.[11] They argued that, unlike particle diffusion in near-homogeneous stationary turbulent flow, the dispersed-phase motion in free shear layers such as mixing layer is governed by the large-scale, rotating structures that represent a quasiorderly (not stochastic) mo-

tion. Thus they suggested that the small-scale local turbulence may cause a local diffusion effect, but the primary dispersion mechanism is the fluid motion due to large-scale turbulent structure. Some simulation results[4,6,9] for particle dispersions in a vortex pair and in a jet have also supported this physical concept. However, the time-dependent methods developed by Crowe's group are based on an initial, idealized vortex distribution (usually by means of acoustic forcing) in flowfield with,[4,6,9] and without,[16] the assumption that the effects of the dispersed phase on the flowfield are neglected. It is well known[12] that the effects of the dispersed phase on the continuous phase are through not only the production of the momentum source term but also the modification of turbulence structure. Furthermore, the experiments conducted by Wang and Liu[10] and Liu[17] revealed that no apparent vortex structure with natural evolution condition was observed in the two-phase mixing layer under the loading of polydispersed-size particles. These results are different from the observations reported by Crowe et al.[11]

Most earlier experimental investigations[3,7,18] in two-phase mixing layer flows focused on the effects of the monodispersed phase on the two-phase flow structure. Very few measurements in relation to the polydispersed properties were reported. According to the numerical studies of Chein and Chung,[4,6] the particles with different Stokes numbers exhibited quite different dispersion rates in the two-phase mixing layer. It is worthwhile to have available experimental data useful for evaluation of the dispersion characteristics in the polydispersed cases of two-phase mixing layer flow. Moreover, none of the existing measurements in two-phase mixing layer flows provide the complete inlet conditions required for the model validation. The present investigation using a relatively new instrumentation, phase Doppler particle analyzer (PDPA), differs from those previous ones in many details, but principally in providing as complete information as possible about the mean and fluctuating properties for both continuous and dispersed phases in mixing layer flow.

The objectives of this study are 1) to provide a well-defined benchmark quality data base useful for model validation and 2) to evaluate the theoretical calculations against the measurements in a two-phase turbulent mixing layer flow with polydispersed drop sizes.

II. Experimental Methods

Test Facility

Experimental works were conducted in a vertical tunnel as shown in Fig. 1. The tunnel was divided into two separate flow paths by a central splitting plate. The contraction ratio for the tunnel was 16:1 with a 150 × 150 mm^2 cross-sectional area at the test section. The turbulence levels were found to be less than 0.5% in the hot-wire measurements (Dantec Model 55M) for both low- and high-speed streams. A Sono-Tek ultrasonic nozzle, located 950 mm upstream of the test section in the high-speed stream, generated the polydispersed drops whose diameters ranged from 3 to 100 μm. The trailing edge of the splitting plate was extended 150 mm into the test section. This configuration allowed the drops to reach dynamic equilibrium with the carrier gas before leaving the splitting plate. Water was used as the atomizing fluid. The Sauter mean diameter and the number density of the water drops were 54 μm and 1200 #/cc, respectively. Experiments were performed under the condition that the mean velocities of the high- and low-speed streams were equal to 10.2 and 2.36 m/s, respectively. A rectangular coordinate (see Fig. 1) is selected such that the streamwise x coordinate is positive downward with the origin at the central separation point of the splitting plate, the transverse y coordinate (normal to the splitting plate) is positive toward the high-speed stream side, and the parallel z coordinate is along the splitting plate. The measurements were made in the x-y plane with $z = 0$. Data were collected at four x stations: 5, 20, 40, and 80 mm from the separation point of the splitting plate. The two-dimensional assumption was insured by the uniformity of the distributions of the streamwise velocity components for both phases along the z direction measured at these four investigated x stations in the plane of $y = 0$.

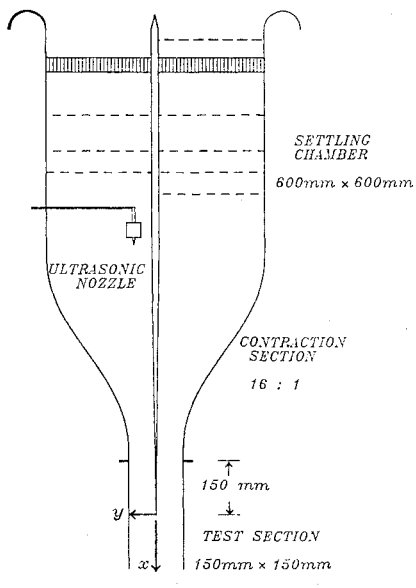

Fig. 1 Schematic of test facility.

Instrumentation

Mean and fluctuating velocities of both phases were measured with a two-component phase Doppler particle analyzer (PDPA, Aerometric, Inc., Model 3200-3). This instrument can simultaneously measure two orthogonal components of velocity and size for individual drops.[19] A smoke generator (using kerosene as the working fluid) was used to generate seeding particles (nominal 0.8 μm) for the velocity measurements of the continuous phase. The PDPA was mounted on a three-axis transverse system that permits positioning to within 0.01 mm. The ensemble-averaged quantities were statistically calculated by collecting 30,000 sample data for each measurement point. The sampling time depended on the local number density of drops. It took about 30 s to collect this number of scattering signals in most regions of the interesting domain. However, the sampling time of 900 s was set as the upper limit to record meaningful data in the measurements. Uncertainties in mean and fluctuating velocities of the continuous phase using the PDPA were within 2% in comparison with the measurements of a pitot tube in the measuring range from 2 to 10 m/s. Repeatabilities in mean and fluctuating velocities of both phases were also within 2% uncertainty under the test conditions. Mass conservation checks for liquid flow rates at each measuring axial station, by comparing with the metered liquid flow rate in the upstream water supply line, revealed that the uncertainty in mean liquid flow flux was at most 10%.

Eight data sets of the dispersed phase with the drop sizes of 10, 20, 30, 40, 50, 60, 70, and 80 μm were recorded in this work. More details of the experimental methods can be found in Ref. 17. The complete information, including the distributions of u, v, u', v', w', $\overline{u'v'}$, u_p^k, v_p^k, G_p^k, and drop size, measured at the streamwise station of $x = 5$ mm, will serve as the inlet conditions required for the theoretical calculation.

III. Theoretical Methods

The boundary-layer assumption for a steady, planar, two-phase mixing layer is used in the analysis. For the present work, since the volumetric fractions occupied by the dispersed phase are equal to or less than the magnitude order of 10^{-5} in the entire computational domain, the two-phase flow can be reasonably considered as a dilute case and the drop-drop interaction is negligible. Further, there are no large-scale structures to be observed in the present (naturally evolving)

two-phase mixing layer as illustrated in Fig. 2a. Analysis of the pressure and velocity data did not reveal any dominant frequency occurring in the two-phase mixing layer with naturally evolving condition either. The side-view photographs of both unforced (naturally evolving) and forced flow visualizations (Figs. 2a and 2b, respectively) were obtained by illuminating the test section with a flashlight (10^{-4} s exposure time) and injecting the smoke particles into the high-speed stream. The motion is from top to bottom. Notice that the quasi-orderly vortex structures as argued by Crowe et al.[11] do appear (see Fig. 2b) when the flow is acoustically forced with a frequency of 140 Hz and level of 80 dB in the settling chamber of the high-speed stream side. However, the problem to be addressed in this work is the natural evolving case and will be formulated, according to the previous discussion in Sec. I, by using the Eulerian-Lagrangian approach.

Continuous Phase Equations

The k-ϵ turbulence model capable of adequately describing the turbulent motion of simple flows such as the present mixing layer is employed for the theoretical study. Since the void fraction of the carrier gas is very close to unity, the governing equations for the continuous phase expressed in a Reynolds-averaged basis can be cast into a general form as follows:

$$\frac{\partial}{\partial x}(\rho u \phi)+\frac{\partial}{\partial y}(\rho v \phi)=\frac{\partial}{\partial y}\left(\Gamma_\phi \frac{\partial \phi}{\partial y}\right)+S_\phi+S_{p\phi} \tag{1}$$

The parameters ϕ, Γ_ϕ, S_ϕ, and $S_{p\phi}$ appearing in Eq. (1) are summarized in Table 1, along with the appropriate empirical constraints.[20] Here $S_{p\phi}$ represents the source term due to the interactions between the continuous and dispersed phases.

Consideration of the effect of the drop dispersion on turbulence yields extra dissipation terms in the modeled equations for k and ϵ. Nevertheless, a reasonable assumption can be made for the present dilute case (maximum volumetric fraction of the dispersed phase is on the order of magnitude of 10^{-5}) that the turbulence modulation effects are negligible. To confirm this inference, calculations were performed by inclusion of the turbulence modulation model developed by Chen and Wood.[21] It was found that numerical values of these extra dissipation terms were usually two to three orders of magnitude less than those for the source terms of S_ϕ listed in Table 1. As a result, the consideration with and without the turbulence modulation effects did not cause any significant change in the resulting numerical solutions. Hence, the terms of $S_{p\phi}$ shown in Eq. (1) for $\phi = k$, ϵ are set to be zero (see Table 1).

Dispersed Phase Equations

The dispersed phase is treated by tracking individual drops as they move through the turbulence field of the continuous phase.[14,15,22] This is essentially a statistical (Monte Carlo) approach and requires the tracking of an adequately great number of computational drops to obtain statistically stationary information for the dispersed phase. Each of these computational drops characterizes a group of physical drops possessing the same size and velocity.

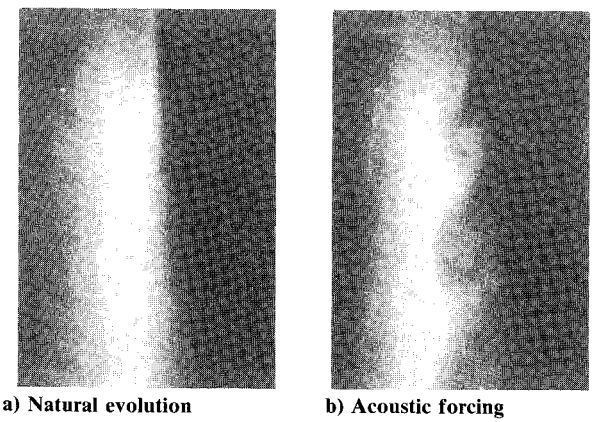

a) Natural evolution b) Acoustic forcing

Fig. 2 Flow visualizations in two-phase planar mixing layer.

Table 1 Governing equations of the continuous phase

ϕ	Γ_ϕ	S_ϕ	$S_{p\phi}$
u	μ_{eff}	0	S_{pu}[a]
v	μ_{eff}	0	S_{pv}[a]
k	$\mu_{\text{eff}}/\sigma_k$	$\mu_t\left(\frac{\partial u}{\partial y}\right)^2-\rho\epsilon$	0
ϵ	$\mu_{\text{eff}}/\sigma_\epsilon$	$C_1\mu_t\frac{\epsilon}{k}\left(\frac{\partial u}{\partial y}\right)^2-C_2\rho\frac{\epsilon^2}{k}$	0
		$\mu_t = C_\mu \rho k^2/\epsilon$	
		$\mu_{\text{eff}} = \mu + \mu_t$	

C_μ	C_1	C_2	σ_k	σ_ϵ
0.09	1.44	1.87	1.0	1.3

[a]Obtained with the PSI-cell method.

The equation of motion for the kth computational drop was originally derived by Basset, Boussinesq, and Oseen and is known as the B-B-O equation. For large drop-to-gas density ratio ($\rho_p/\rho \simeq 900$ in this work), effects of static pressure gradients, virtual mass, Basset, and Magnus forces can be neglected with little errors. Associated with the previously stated assumptions, the B-B-O equation of the kth computational drop in the ith direction becomes

$$\frac{dU_{pi}^k}{dt}=\frac{U_i-U_{pi}^k}{\tau_p^k}+g_i \tag{2}$$

where

$$\tau_p^k=\frac{4d_p^k\rho_p}{3C_D^k\rho|\underline{U}-\underline{U}_p^k|} \tag{3}$$

and

$$U_i = u_i + u_i' \tag{4}$$

Note that the velocities shown in the previous equations denote instantaneous velocities. The drag coefficient for a spherical drop is given by an empirical formula[23]:

$$C_D^k=\frac{24}{Re^k}\left[1+\frac{(Re^k)^{2/3}}{6}\right], \qquad Re^k \le 1000$$
$$= 0.44, \qquad Re^k > 1000 \tag{5}$$

where the drop Reynolds number is defined by

$$Re^k = \rho|\underline{U}-\underline{U}_p^k|d_p^k/\mu \tag{6}$$

The trajectory of the kth computational drop is determined by directly integrating its velocity with respect to time.

Drops are assumed to interact with an eddy in a turbulent field for a time that is determined as the smaller of the eddy lifetime τ_e and the residence time of the kth computational drop in the eddy τ_r^k. Hence, to insure the drop-eddy interaction, the integrating time step Δt must satisfy the following criteria:

$$\Delta t \le \min(\tau_e, \tau_r^k) \tag{7}$$

If the characteristic size of an eddy is assumed to be its dissipation scale L_e given by

$$L_e = C_l^{3/4}\mu k^{3/2}\epsilon \tag{8}$$

the eddy lifetime is then estimated as[22]

$$\tau_e = L_e / |\underline{u}'| \tag{9}$$

The residence time of the kth computational drop in the eddy is obtained from

$$\tau_r = L_e / |\underline{U} - \underline{U}_p^k| \tag{10}$$

IV. Numerical Solution Procedure and Boundary Conditions

Equation (1) is solved using the finite-volume method. The characteristics of parabolic differential equations embedded in Eq. (1) allow the employment of the upwind scheme[24] along the marching (streamwise) direction. The power-law scheme[24] is employed for calculation of the convection-diffusion terms along the transverse direction. The calculations are performed using 52 transverse grid nodes with adaptive distribution and marching step size limited by 3% of the transverse grid width.[22] Numerical tests revealed that a nearly grid-independent solution was obtained with this kind of grid layout.

Since the relationship $\overline{u'^2}:\overline{v'^2}:\overline{w'^2} = 1:½:½$ is approximately valid in the measurements of the present work, velocity fluctuations are assumed to be in the Gaussian form having the standard deviations of $\sqrt{k}$, $\sqrt{k/2}$, and $\sqrt{k/2}$ for u', v', and w', respectively. The fluctuating velocity component u_i' is chosen randomly from its corresponding probability density function (PDF) at each integrating time step Δt. Hence, for a given u_i', there exists a corresponding value of PDF, P. To obtain a statistically stationary solution, eight groups of different drop diameters, each being divided into 1500 computational drops, are employed in the calculations.

The instantaneous velocity components of the dispersed phase are determined by iteratively integrating the nonlinear ordinary differential equation of Eq. (2) to an acceptable tolerance in a given time step. The mean value of the dispersed-phase velocity at a specified grid node is calculated by using the ensemble-averaging concept:

$$u_{pi} = \sum_{m=1}^{M} n_m P_m U_{pi}^m / \sum_{m=1}^{M} n_m P_m \tag{11}$$

where the index m denotes the mth computational group passing through the crossing surface normal to the direction i at a specified grid node.

The source terms due to two-phase interactions $S_{p\phi}$ in the continuous-phase momentum equations (see Table 1) are obtained using the PSI-cell method suggested by Crowe et al.[25] These source terms are then used in the next global iteration of the continuous-phase flowfield until convergence is attained. The criterion based on the normalized momentum residual is set to be 10^{-8} for monitoring convergence of all continuous-phase governing equations.

At the inlet station of $x = 5$ mm, all of the required information except ϵ are specified using the measured data. However, the required ϵ information at the inlet station can be obtained by combining the Boussinesq hypothesis and relationship of the eddy viscosity between k and ϵ. The shear stress $\overline{u'v'}$ measured at the inlet station is expressed by

$$-\rho\overline{u'v'} = \mu_t\left(\frac{\partial u}{\partial y} + \frac{\partial v}{\partial x}\right) \tag{12}$$

Introduction of the definition of the eddy viscosity (see Table 1) into Eq. (12) yields

$$\epsilon = -C_\mu k^2\left(\frac{\partial u}{\partial y} + \frac{\partial v}{\partial x}\right) \Big/ \overline{u'v'} \tag{13}$$

To estimate the value of $\partial v/\partial x$, measurements of v were also made at the station of $x = 6$ mm. The ϵ information is calculated using the measured u, v, k, and $\overline{u'v'}$ in the work. It is noted that the calculated ϵ profile can be approximately expressed in the following form by the best comparison with the prediction of Eq. (13):

$$\epsilon = C\mu k^{3/2}/(0.048b) \tag{14}$$

where b denotes the mixing layer width at the inlet station defined by the following expression:

$$b = y_{0.95} - y_{0.1} \tag{15}$$

The transverse characteristics $y_{0.95}$ and $y_{0.1}$ are the transverse positions where the values of $(u - u_{-\infty})/(u_{+\infty} - u_{-\infty})$ are equal to 0.95 and 0.1, respectively. The value of b, calculated from Eq. (15) with the measured u profiles at the inlet station, is equal to 7 mm in the present work.

Two entrainment boundary conditions are represented by $d\phi/dy = 0$ instead of $\phi = 0$ at the sufficiently far transverse distances in the high-speed stream side ($y_{+\infty}$) and the low-speed stream side ($y_{-\infty}$), separately. Numerical tests revealed that $y_{+\infty} = 34$ mm and $y_{-\infty} = -17$ mm were the sufficiently far transverse distances in the high- and low-speed stream sides, respectively, to satisfy the entrainment boundary conditions in the computational domain of this work.

V. Results and Discussion

The evolution of the predicted and measured mean streamwise and mean transverse velocity components of the continuous phase are plotted in Figs. 3a and 3b, respectively. Note that these two figures are presented in different velocity scales. It is observed that wake exists in the upstream region ($x = 5$ mm) but disappears in the regions behind $x = 20$ mm. Figure 3b shows clearly the flow entrainment into the mixing region from both high-and low-speed stream sides. Further, the momentum transfer rate along the transverse direction from the high-speed stream side to the mixing region is higher than that from the low-speed stream side.

The momentum thickness, which characterizes the transverse length scale of the mixing region, is defined by

$$\theta = \int_{y-\infty}^{y+\infty} \frac{(u_{+\infty} - u)(u - u_{-\infty})}{(u_{+\infty} - u_{-\infty})^2}\,dy \tag{16}$$

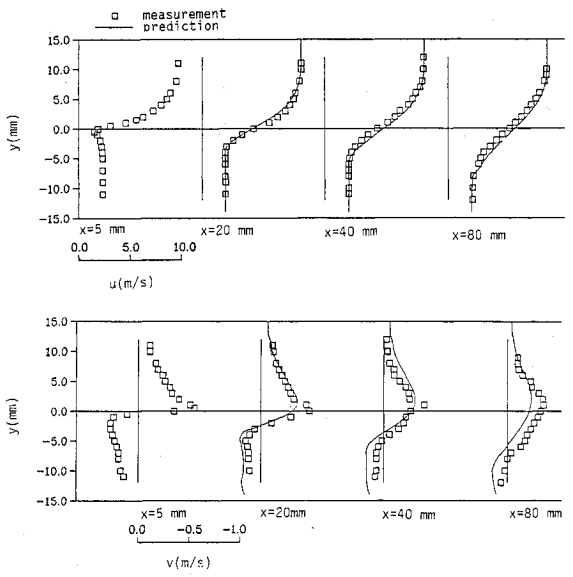

Fig. 3 Evolution of the predicted and measured a) mean streamwise velocity components and b) mean transverse velocity components of the continuous phase.

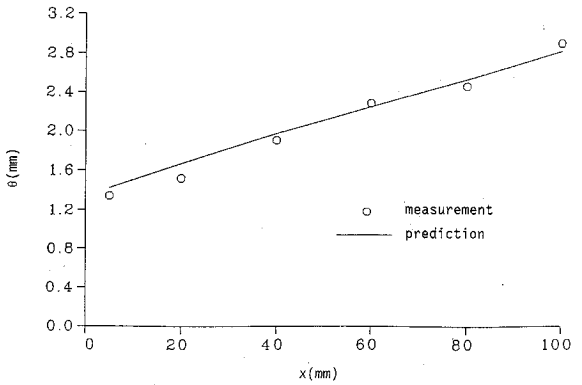

Fig. 4 Comparison of the predicted and measured momentum thickness of the mixing layer.

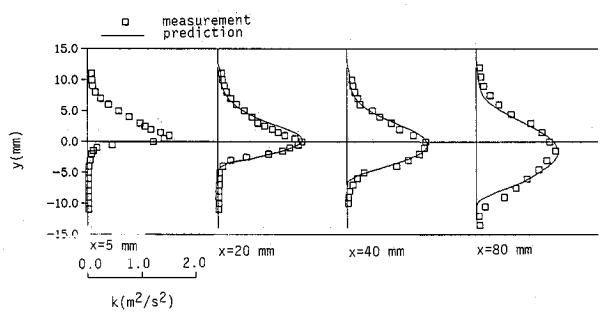

Fig. 5 Evolution of the predicted and measured turbulent kinetic energy of the continuous phase.

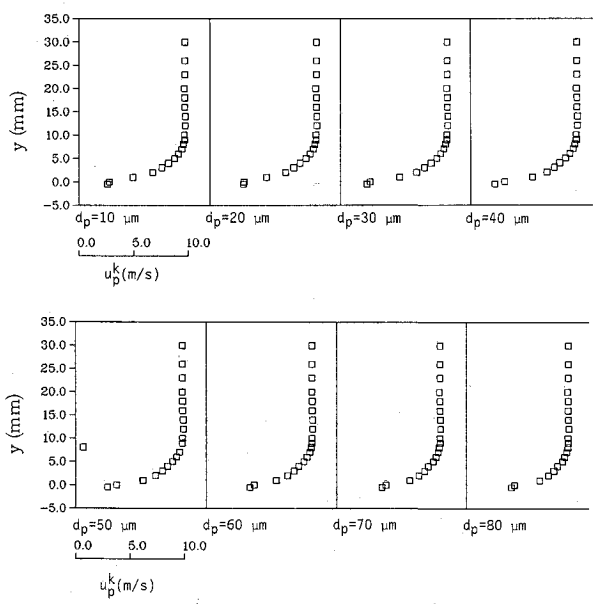

Fig. 6 Measured profiles of the mean streamwise velocity component of the drops with sizes of 10, 20, 30, 40, 50, 60, 70, and 80 μm at the station of $x = 5$ μm.

Figure 4 shows comparisons between predicted and measured values of the momentum thickness. It is known[26] that the vortex merging process significantly enhances the growth of the mixing layer. However, as shown in Fig. 2a, no apparent vortex formation is observed in this natural evolving case. This primarily leads to an approximately 44% reduction of the momentum thickness of the present two-phase case in comparison with the homogeneous case as indicated in Ref. 17.

The evolution of the predicted and measured turbulent kinetic energy of the continuous phase is plotted in Fig. 5. Obviously, the peak values move from the high-speed stream side in the upstream region to the low-speed stream side in the downstream region. This might be explained by the fact that the momentum transport from the high-speed stream side to the mixing region is higher than that from the low-speed stream side as revealed from Fig. 3b. It is also noted from Refs. 10 and 17 that the k values in the two-phase case are smaller than those in the homogeneous phase case, which is consistent with observations obtained by Hetsroni and Sokolov[27] as well as Modarress et al.[28] in free shear flows. Turbulence attenuation due to the existence of drops in the two-phase case also causes the slow development of the momentum thickness in comparison with the homogeneous phase case (see Refs. 10 and 17) as argued before.

In general, the theoretical predictions of the continuous phase are in good agreement with the measurements.

As mentioned in Sec. II, eight discrete drop sizes were employed in this work to simulate the spectral effects of the size distribution in the spray. For the sake of abbreviation, only the results with the sizes of 20, 40, and 80 μm representing small, medium, and large drops are reported here. Nevertheless, to provide complete initial conditions of the dispersed

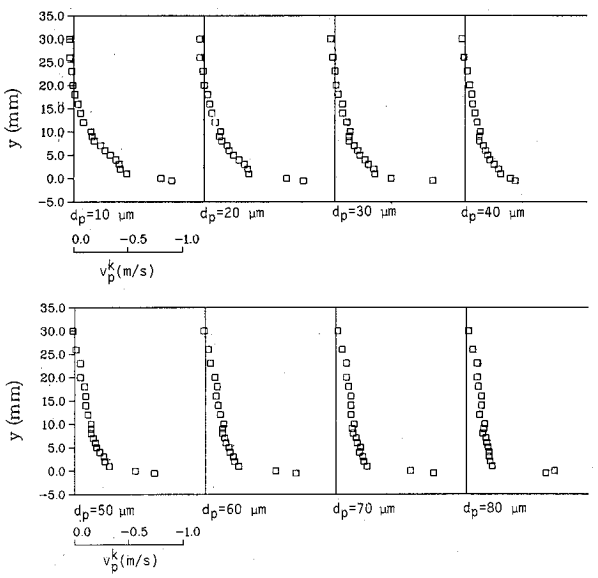

Fig. 7 Measured profiles of the mean transverse velocity component of the drops with sizes of 10, 20, 30, 40, 50, 60, 70, and 80 μm at the station of $x = 5$ mm.

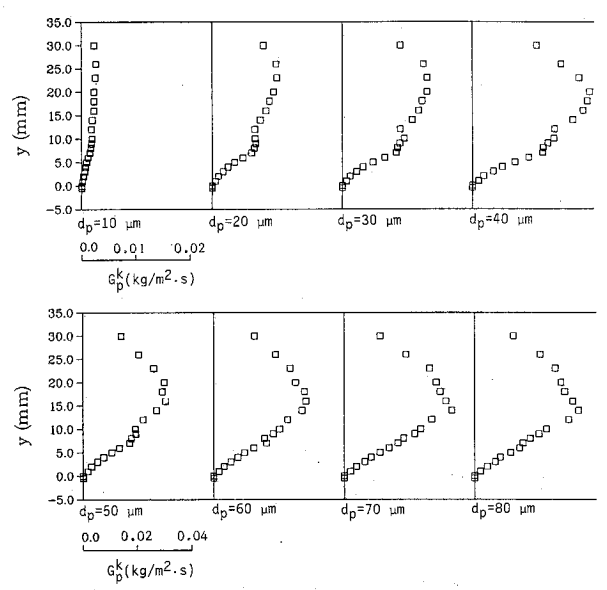

Fig. 8 Measured profiles of the mean liquid fluxes of the drops with sizes of 10, 20, 30, 40, 50, 60, 70, and 80 μm at the station of $x = 5$ mm.

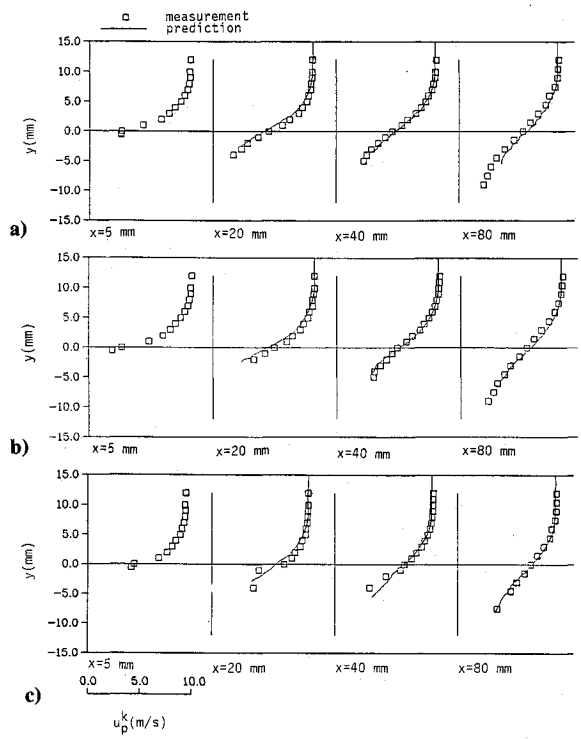

Fig. 9 Evolutions of the predicted and measured mean streamwise velocity components of the drops with sizes of a) 20 μm, b) 40 μm, and c) 80 μm.

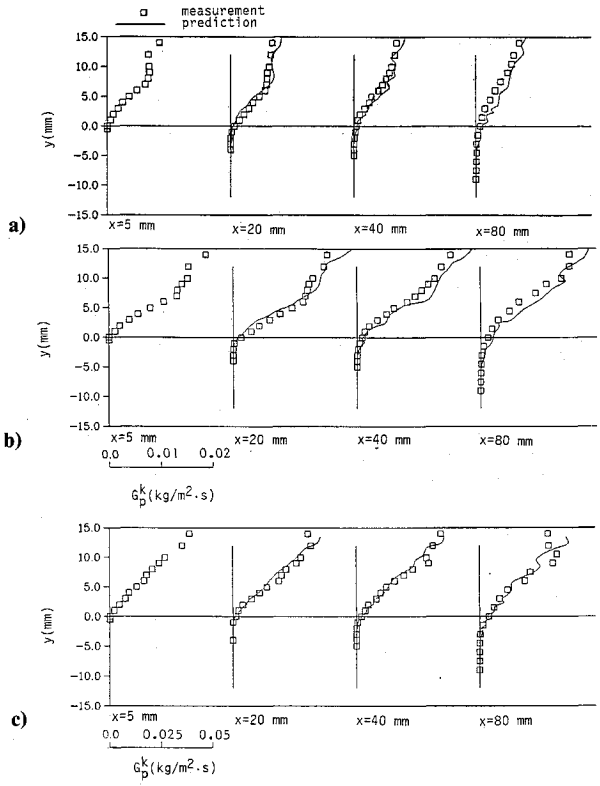

Fig. 10 Comparisons of the predicted and measured mean liquid fluxes of the drops with sizes of a) 20 μm, b) 40 μm, and c) 80 μm.

phase required for calculation, the measured profiles of mean streamwise velocity component, transverse velocity component, and liquid mass flux for the eight discrete drop sizes at the station of $x = 5$ mm are presented in Fig. 6, 7, and 8, respectively.

The evolutions of the predicted and measured mean streamwise velocity component with these three drop sizes are shown in Fig. 9. Comparisons between the predictions and measurements displayed in Fig. 9 are generally in good agreement except for the drop penetration depth into the low-speed stream side due to the turbulent dispersion. It is known that the turbulent dispersion effect on trajectory determination of large drops is more dominated by their inherent inertia. The predictions shown in Fig. 9 do exhibit this trend. For the drops with 80 μm size (Fig. 9c), the predicted deepest positions where the drops can reach in the low-speed stream side are consistent with the experimental observations. However, for the drops with sizes of 20 μm (Fig. 9a) and 40 μm (Fig. 9b), the predicted penetration depths in the low-speed stream side are shorter than the experimental observations, particularly in the downstream regions. Theoretically, the random selection of u_i' can be made from $-\infty$ to $+\infty$, but the limited computer capacity restricts u_i' in a finite range. In the present calculation, values of u_i' were bounded in ± 1.5 times its corresponding standard deviation. If the bounded range of u_i' was enlarged, the drop dispersion effect could be better represented in the calculation. In other words, the penetration depth of small drops in the low-speed stream side could be improved. Nevertheless, the employment of a wider bounded range would need more computational drops and, consequently, more computer efforts to obtain a statistically stationary solution.

Figure 10 shows comparisons between predicted and measured mean liquid mass fluxes (G_p^k) with the sizes of 20, 40, and 80 μm. If Figs. 10a and 10b are compared with Figs. 9a and 9b, respectively, one could observe that, in the low-speed stream regions where the predicted drop trajectories cannot reach by using the present calculation method, the measured mean values of liquid mass fluxes have almost dropped to zero; that is, the number of drops to be sampled is negligibly small. This indicates that the prediction deviations stemming from the present calculation method do not cause any significant change in the simulation of two-phase flow structure.

The evolutions of the predicted and measured mean transverse velocity components with the three selected drop sizes are presented in Fig. 11. Note that the velocity scale demonstrated in Fig. 11 is one order of magnitude smaller than that in Fig. 9. It can be seen from Figs. 11a and 11b that the values

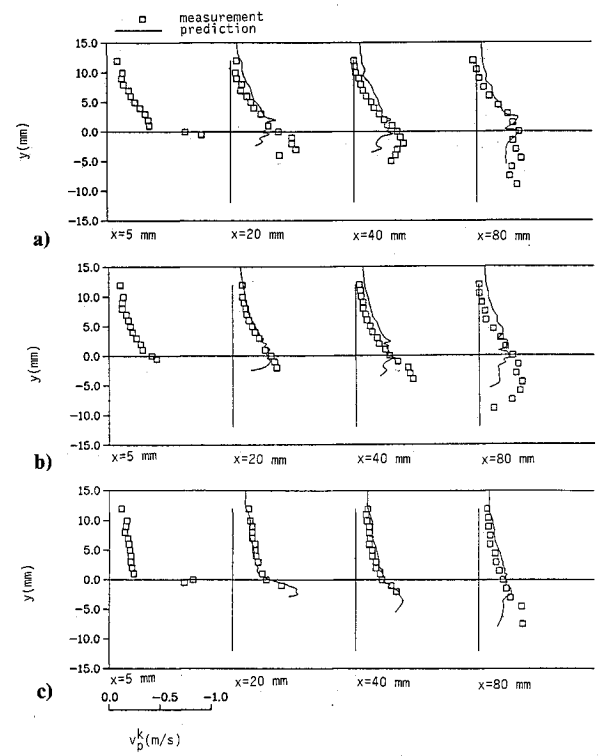

Fig. 11 Evolutions of the predicted and measured mean transverse velocity components of the drops with sizes of a) 20 μm, b) 40 μm, and c) 80 μm.

of the dispersed-phase transverse velocity component are underpredicted in the low-speed stream side as compared with the measurements. As was argued before, this might be attributed to the employment of the relatively narrow bounded range of v' in the present calculation. This underprediction extent seems to be alleviated for the large drop size (see Fig. 11c) owing to the less sensitivity to turbulent dispersion effect. However, the apparent underprediction is also observed in the downstream station of $x = 80$ mm for the computational drops with 80 μm size. The underpredictions of the dispersed-phase transverse velocity component in the low-speed stream side revealed from Figs. 11a and 11b also explain a fact of shorter predicted penetration depths for the computational drops with 20 and 40 μm sizes as discussed before.

VI. Conclusions

A detailed well-defined data set useful for model validation in a two-phase mixing layer flow with polydispersed drop sizes is presented. Complete initial conditions required for theoretical calculation were provided with measurements to avoid prediction uncertainty introduced from the usual assumptions of initial conditions.

Theoretical investigation is performed with the Eulerian-Lagrangian formulation in association with the k-ϵ turbulence model. The accuracy of the theoretical predictions of a two-phase structure has been assessed by the measured data. The comparisons show that the predictions with the present Eulerian-Lagrangian model for a dilute two-phase flow yield reasonable agreement with the measured data. Some prediction deviations such as the penetration depths of small drops caused by turbulence dispersion effects are primarily attributed to the employment of narrower bounded range of u_i' in the Monte Carlo calculation procedure.

Acknowledgment

This work was sponsored by the National Science Council of the Republic of China under Contract NSC-79-0401-E006-32.

References

[1]Brown, G. L., and Roshko, A., "Density Effects and Large-Scale Structures in Two-Dimensional Mixing Layer," *Journal of Fluid Mechanics*, Vol. 64, Pt. 4, 1974, pp. 775–816.

[2]Winant, C. D., and Browand, F. K., "Vortex Pairing, the Mechanism of Turbulent Mixing Layer Growth at Moderate Reynolds Numbers," *Journal of Fluid Mechanics*, Vol. 63, Pt. 2, 1974, pp. 237–255.

[3]Kamalu, N., Wen, F., Troutt, T. R., and Crowe, C. T., "Particle Dispersion by Ordered Motion in Turbulent Mixing Layers," *ASME Cavitation and Multiphase Flow Forum*, FED Vol. 64, American Society of Mechanical Engineers, New York, 1987, pp. 150–154.

[4]Chein, R., and Chung, J. N., "Effects of Vortex Pairing on Particle Dispersion in Turbulent Shear Flows," *International Journal of Multiphase Flow,* Vol. 13, No. 6, 1987, pp. 785–802.

[5]Sabnis, J. S., Choi, S. K., Buggeln, R. C., and Gibeling, H. J., "Computation of Two-Phase Shear-Layer Flow Using an Eulerian-Lagrangian Analysis," AIAA Paper 88-3202, Jan. 1988.

[6]Chein, R., and Chung, J. N., "Simulation of Particle Dispersion in a Two-Dimensional Mixing Layer," *AIChE Journal*, Vol. 34, No. 6, 1988, pp. 946–954.

[7]Kobayashi, H., Masutani, S. M., Azuhata, S., and Hishinuma,Y., "Dispersed Phase Transport in a Plane Mixing Layer," *Transport Phenomena in Turbulent Flow—Theory, Experiment and Simulation*, Hemisphere, New York, 1988, pp. 433–446.

[8]Lazaro, B. J., and Lasheras, J. C., "Particle Dispersion in a Turbulent, Plane Shear Layer," *The Physics of Fluids A*, Vol. 1, No. 6, 1989, pp. 1035–1044.

[9]Yang, J., Chung, J. N., Troutt, T. R., and Crowe, C. T., "The Influence of Particles on the Spatial Stability of Two-Phase Mixing Layers," *The Physics of Fluids,* Vol. 2, No. 10, 1990, pp. 1839–1845.

[10]Wang, M. R., and Liu, Y. C., "Behavior of Polydispersed Sprays in a Plane Mixing Layer," *ASME Forum on Turbulent Flows* (Portland OR), FED Vol. 112, American Society of Mechanical Engineers, New York, June 1991, pp. 69–73.

[11]Crowe, C. T., Chung, J. N., and Troutt, T. R., "Particle Mixing in Free Shear Flows," *Progress in Energy and Combustion Science*, Vol. 14, No. 3, 1988, pp. 171–194.

[12]Faeth, G. M., "Mixing, Transport and Combustion in Sprays," *Progress in Energy and Combustion Science*, Vol. 13, No. 4, 1987, pp. 293–345.

[13]Durst, F., "Eulerian and Lagrangian Predictions of Particulate Two-Phase Flows: A Numerical Study," *Applied Mathematical Modelling*, Vol. 8, April 1984, pp. 101–114.

[14]Mostafa, A. A., and Mongia, H. C., "On the Modeling of Turbulent Evaporating Sprays: Eulerian Versus Lagrangian Approach," *International Journal of Heat and Mass Transfer*, Vol. 30, No. 12, 1987, pp. 2583–2593.

[15]Adeniji-Fashola, A., and Chen, C. P., "Modeling of Confined Turbulent Fluid-Particle Flows Using Eulerian and Lagrangian Schemes," *International Journal of Heat and Mass Transfer*, Vol. 33, No. 4, 1990, pp. 691–701.

[16]Tang, L., Crowe, C. T., Chung, J. N., and Troutt, T. R., "A Numerical Model for Droplets Dispersing in a Developing Plane Shear Layer Including Coupling Effects," *Numerical Methods for Multiphase Flows,* FED Vol. 91, American Society of Mechanical Engineers, New York, 1990, pp. 27–33.

[17]Liu, Y. C., "Transition of the Plane Mixing Layer Under Particle Loading," Ph.D. Thesis, Inst. of Aeronautics and Astronautics, National Cheng-Kung Univ., Tainan, Taiwan, ROC, 1991.

[18]Kamalu, N., Tang, L., Troutt, T. R., Chung, J. N., and Crowe, C. T., "Particle Dispersion in Developing Shear Layer," *Proceedings of International Conference on Mechanics of Two-Phase Flows*, National Taiwan University, Taipei, Taiwan, June 1989, pp. 199–202.

[19]Bachalo, W. D., and Houser, M. M., "Phase Doppler Spray Analyzer for Simultaneous Measurements of Drop Size and Velocity Distributions," *Optical Engineering,* Vol. 23, No. 5, 1984, pp. 583–590.

[20]Shearer, A. J., Tamura, H., and Faeth, G. M., "Evolution of a Locally Homogeneous Flow Model of Spray Evaporation," *Journal of Energy*, Vol. 3, Sept.-Oct. 1979, pp. 271–278.

[21]Chen, C. P., and Wood, P. E., "A Turbulence Closure Model for Dilute Gas Particle Flows," *The Canadian Journal of Chemical Engineering,* Vol. 63, June 1985, pp. 349–360.

[22]Shuen, J.-S., Soloman, A. S. P., Zhang, Q.-F., and Faeth, G. M., "Structure of Particle-Laden Jets: Measurements and Predictions," *AIAA Journal*, Vol. 23, No. 3, 1985, pp. 396–404.

[23]Putnam, A., "Integratable Form of Droplet Drag Coefficient," *ARS Journal*, Vol. 31, Oct. 1961, pp. 1467, 1468.

[24]Patankar, S. V., *Numerical Heat Transfer and Fluid Flow,* McGraw-Hill, New York, 1980, Chap. 5.

[25]Crowe, C. T., Sharma, M. P., and Stock, D. E., "The Particle-Source-In Cell Model for Gas-Droplet Flows," *ASME Journal of Fluid Engineering*, Vol. 99, June 1977, pp. 325–332.

[26]Browand, F. K., and Latigo, B. O., "Growth of the Two-Dimensional Mixing Layers from a Turbulent and Nonturbulent Boundary Layer," *The Physics of Fluids*, Vol. 22, No. 6, 1979, pp. 1011–1019.

[27]Hetsroni, G., and Sokolov, M., "Distribution of Mass, Velocity and Intensity of Turbulence in a Two-Phase Turbulent Jet," *ASME Journal of Applied Mechanics*, Vol. 38, No. 2, 1971, pp. 315–327.

[28]Modarress, D., Tan, H., and Elghobashi, S., "Two-Component LDV Measurement in a Two-Phase Turbulent Jet," *AIAA Journal*, Vol. 22, No. 5, 1984, pp. 624–630.